Global NEST Journal, Vol 26, No 3, 05681


# Photocatalysis technology for treating petroleum wastewater and the potential application of tapered bubble column (TBC): a review

**Firdos M. Abdulla[1], Z.Y. Shnain[2], A.A. Alwasiti[3], M.F. Abid[4] and N.H. Abdurahman[5]**
[1,2,3]Department of Chemical Engineering, University of Technology (UOT), Baghdad, Iraq
[4]Department of Oil & Gas Refining Engineering, Al-Turath University College, Baghdad, Iraq
[5]Faculty of Chemical and Natural Resources Engineering, University Malaysia Pahang-UMP
Received: 02/02/2019, Accepted: 17/03/2020, Available online: 27/05/2020
*to whom all correspondence should be addressed: e-mail: firdos.m.abdulla@uotechnology.edu.iq
https://doi.org/10.30955/gnj.003058

**Graphical abstract**

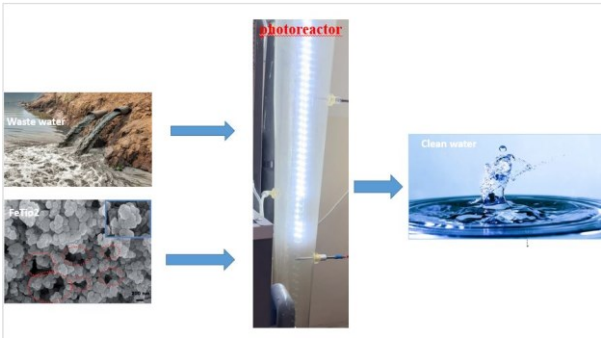


**Abstract**

The photocatalytic oxidation of organic and petroleum wastewater treatment is an advanced oxidation process (AOP) with several benefits. It operates at normal temperatures and pressure, is inexpensive, does not produce secondary waste, and us easily accessible. Many studies have employed bubble columns, slurry bubble columns, and three-phase fluidized reactors in the photocatalytic process for wastewater treatment. Pure $TiO_2$ and Fe-doped $TiO_2$ are considered the most promising catalysts. The aim of this work is to review the main factors affecting the photocatalytic process of organic pollutants and petroleum wastewater (produced water) treatment, photocatalysts type, with a special focus on pure $TiO_2$ and Fe-doped $TiO_2$, light source, and reactor type.

**Keywords**: Photocatalysis, produced water, Fe doped $TiO_2$, Tapered bubble column.

## 1. Introduction

Produced water (petroleum wastewater) consists of a wide variety of pollutants, including oil and grease; alkanes; olefins; polycyclic aromatic hydrocarbons (PAHs); benzene, toluene, and xylene (BTX); mercaptans; phenol; ammonia; and many other organic compounds, in addition to a high level of total solids, and high biochemical oxygen demand (BOD) and chemical oxygen demand (COD) (Varjani *et al.* 2019; Al-Nuaim *et al.* 2022; Al-Nuaim *et al.* 2023).

Treating petroleum refinery wastewater or produced water (PW) requires numerous steps. Figure 1 shows these treatment steps with their objectives (Diya'uddeen *et al.* 2011; Varjani *et al.* 2019).

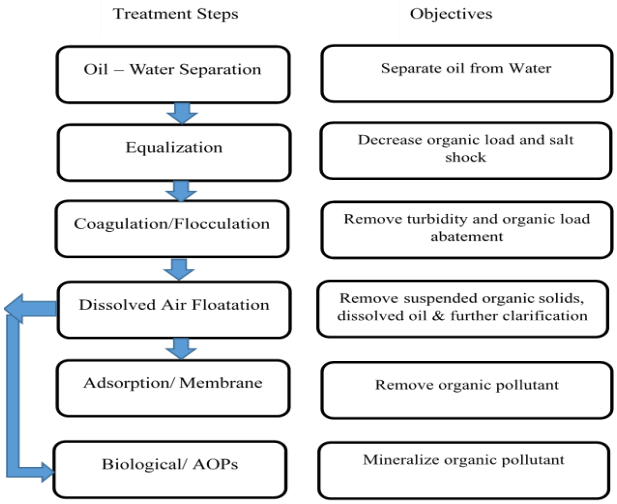


**Figure 1.** General steps and objectives for treating petroleum wastewater (Diya'uddeen *et al.* 2011; Varjani *et al.* 2019).

The four advanced final wastewater treatment processes are adsorption, membrane, biological, and advanced oxidation processes (AOPs). Adsorption and membrane processes transfer the pollutants to different concentrated forms, whereas biological and advanced oxidation processes can mineralize most of the pollutants (Kaur *et al.* 2016; Li *et al.* 2022; Oliveira *et al.* 2022). Table 1 likely provides a comprehensive overview of the four pollution-control methods, highlighting the advantages and disadvantages of each (Chen *et al.* 2020).

Comparing photocatalytic wastewater treatment with other processes, it is considered a promising and it has gained significant attention owing to its many advantages, making it a contemporary and environmentally friendly technology. Some key features of this approach include excellent performance, operation at ambient pressure and temperature, low costs, and the absence of secondary waste formation. Additionally, operating at ambient pressure and temperature makes it a convenient and

energy-efficient method. (Butkovskyi *et al.* 2017; Dewil *et al.* 2017).

Photocatalysis is used to oxidize refractory organic compounds that cannot be oxidized during biological treatment. Many research articles of photolytic degradation performed for treating petroleum wastewater and organic effluents (Varjani *et al.* 2019).

**Table 1.** Comparison of the treatment processes for organic pollutants (Chen *et al.* 2020).

| Process type | Strength | Weakness |
|---|---|---|
| Biological treatment | 1. Cost-effective the environmentally friendly 4nct. | 1. It is not sufficiently copiable to remove a significant amount of organic waste. |
| | 2. Excellent odor and color reduction. | 2. Biosocial systems are difficult to control. |
| | 3. maximum output. | 3. It maintains the chemical oxygen demand values at their current levels. |
| | | 4. Some organic compounds, such as day, have a weak capacity for biodegradation. |
| Chemical precipitation | 1. Energy use control. | 1. High chemical consumption (e.g., lime, oxidants, H2S, etc.) |
| | 2. Easy process. | 2. The pH level must be checked. |
| | 3. There is a wide range of compounds that are readily available in commerce. | 3. There is a lot of sludge produced |
| | 4.Efficient removal of absorbable organic halogen and total organic carbon, particularly in the pulp and paper industries. | 4.The addition of non-recyclable chemicals (coagulants, flocculants, and chemicals) was necessary. |
| Membrane filtration | 1. Quick and effective. | 1. Relatively high operation and maintenance costs |
| | 2.Eco-friendly. Safe for plants and animals, non-toxic, and non-corrosive. | 2. Restricted feeding rate |
| | 3. a high constituent removal rate. | 3.Membrane fouling reduces permeating flux and production. |
| Traditional photocatalysis | 1. It is ecologically sound. | 1. Recovering and regenerating materials is challenging |
| | 2. Excellent susceptibility, high energy efficiency, and low process cost. | 2. Because there are too many pollutants, degradation efficiency decreases. |
| | 3.Catalyst loading adjustments are simple. | 3. Potential photocatalyst losses in long-term use. |

The main advantages of the photocatalytic oxidation can be summarized as follows: (Gogate and Pandit 2004) :

1. Operation occurs at room temperature and pressure.
2. $TiO_2$ is inexpensive, and sunlight can be used with considerable economic savings.
3. $TiO_2$ in aqueous media is chemically stable at a wide range of pH levels (i.e., 0-14).
4. The system requires only low concentrations of $TiO_2$ and no additives.
5. There is a high capacity for recovering noble metals.
6. Many pollutants successfully attain total mineralization.
7. This process is effective with chemicals containing halogens, which are extremely hazardous to bacteria when used in biological water treatment.

The disadvantages of photocatalytic oxidation are outlined in below: (Gogate and Pandit 2004):

1. Reactors cannot be used effectively at industrial scales due to a lack of engineering design and operation procedures. Being unable to evenly irradiate the entire catalyst surface with the same incident intensity presents the greatest challenge when developing large-scale reactors. Opacity, light scattering, depth of radiation penetration, and volumetric light absorption are all factors that limit the scale-up.
2. Chemical reactions during photocatalysis are often slower than with traditional methods, necessitating the use of additional active catalysts in the reactor. The quantity of active catalyst that can be contained in supported reactors is only limited by the thickness of the coating that can be applied to their surface; the more coating, the lower the total conversion efficiency.
3. Separation is very difficult in the suspended catalyst process.
4. There have been few applications to real industrial effluents with high destruction efficiency using photocatalytic oxidation alone.
5. Over time, the degradation rates decrease because the photocatalyst becomes corroded from prolonged use.

The photocatalytic process is made up of three main related components: the photocatalyst, the light source, and the photocatalytic reactor as depicted in Figure 2.

In the context of water treatment, photocatalysis involves the use of photocatalysts, often semiconductor materials like titanium dioxide, which, when illuminated with light, generate reactive oxygen species capable of breaking down pollutants in water. This process is particularly effective

against organic pollutants and can contribute to the degradation of various contaminants (Sajda *et al.* 2024).

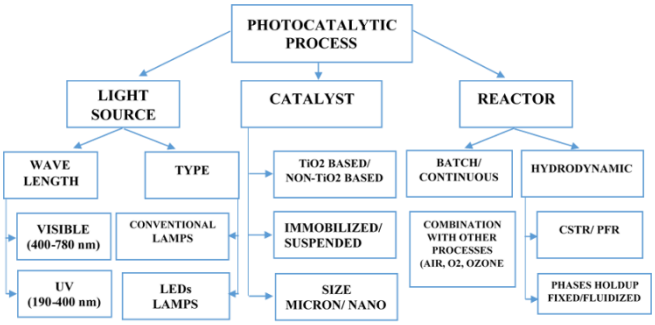


**Figure 2**. General outline of the photocatalytic process.

$TiO_2$-based photocatalysts are commonly used to treat organic pollutants and petroleum industry wastewater. Due to its high catalytic efficiency, stability, and nontoxicity, the $TiO_2$/UV technique has generated a great deal of attention in the field of photocatalysis. It provides the complete mineralization of wastewater from the petroleum industry while maintaining low costs, quick reaction times, no sludge generation, and ease of operation (Al-Nuaim *et al.* 2022; Elmobarak *et al.* 2021; Varjani *et al.* 2019; Ani *et al.* 2018; Aljuboury *et al.* 2017).

Pure $TiO_2$ has a bandgap of 3.2 and 3.6 eV for the crystal types anatase and rutile, respectively. The efficiency of absorption of sunlight is very low, and photocatalysis requires UV light. Doping with different transition metal ions (i.e., Cr, Fe, V, Mn, Co, and Ni) enhances the electrochemical and photochemical activities, introducing new energy levels into the bandgap and decreasing the gap to the visible range (Jeon *et al.* 2000; Zhang *et al.* 2009; Singh *et al.* 2016; Peng *et al.* 2012; Nair *et al.* 2014; Devi *et al.* 2017; Manzoor *et al.* 2018; Marami *et al.* 2018; Xu *et al.* 2018; Drozd *et al.* 2019; Sacco *et al.* 2019a; Chatrnoor *et al.* 2023; Heda *et al.* 2023). Hence, $TiO_2$ based photocatalysts can be divided according to their composition into pure $TiO_2$ and element doped-$TiO_2$ or composite catalyst. The catalyst $TiO_2$ doping with Fe enhances electrochemical and photochemical activities (Chatrnoor *et al.* 2023; Heda *et al.* 2023).

The pollutant, active catalyst, and effective source of illumination must all be in proximity to one another for the photocatalysis to be effective (Ibhadon and Fitzpatrick 2013; Ahmad *et al.* 2016; Oliveira *et al.* 2022).

Many studies have used bubble columns, slurry bubble columns, and three-phase fluidized reactors in the photocatalytic process for wastewater treatment (Cassano and Alfano 2000; (Pozzo *et al.* 2006).

The aim of this work is to highlight the main three factors that effect on photocatalytic oxidation process; catalyst type, light source and reactor type. Furthermore, the article concentrated on the $TiO_2$-based photocatalytic oxidation process for organic pollutants and petroleum wastewater (produced water) treatment, with a special focus on pure $TiO_2$ and Fe-doped $TiO_2$

## 2. Photocatalysts

Advanced oxidation processes (AOPs) for wastewater treatment include a wide variety of chemical processes, of which one is the photocatalytic process. It is employed to remove organic (and sometimes inorganic) pollutants from wastewater by oxidizing them through reactions with the generated hydroxyl radicals (*OH) (Ghime and Ghosh 2020).

Among the several semiconductor photocatalysts, TiO2 is the most widely used. Many scientists are paying closer attention to it because of its many good qualities, which include high oxidation capacity, photo-stability, chemical stability, abundance, low toxicity, low cost, and long-term photostability (Elgohary *et al.* 2021). $TiO_2$-based photocatalysts can be divided according to their composition into pure $TiO_2$ and element doped-TiO2 or composite catalysts. $TiO_2$ doped with Fe enhances the electrochemical and photochemical activities (Chatrnoor *et al.* 2023; Heda *et al.* 2023).

Rutile, anatase, and brookite are the three forms of crystals found in $TiO_2$. The creation of $TiO_2$ particles can be accomplished in a variety of ways, including flame aerosol synthesis (Bettini *et al.* 2016), hydrothermal synthesis (Corradi *et al.* 2005), and sol–gel synthesis (Gotić *et al.* 1996). While retaining the drawbacks of high temperature synthesis, the key benefit of flame aerosol synthesis is its simplicity, but $TiO_2$ crystalline powder is created by hydrothermal synthesis. The lack of a full understanding of the many factors that have a significant impact on photocatalytic performance (i.e., chemical equilibrium, nucleation kinetics, and phase growth) makes it difficult to regulate the overall process. The porous structure of the $TiO_2$ materials, which lowers the hydraulic resistance of $TiO_2$ films and increases their photocatalytic activity, is a crucial component of sol-gel chemistry synthesis (Li *et al.* 2022).

Photocatalytic systems are typically configured in one of the following ways:

### *2.1. Tio₂ powder suspension photocatalytic process*

High-contact surface area, which results in a quicker reaction time and easier operation, is a defining feature of slurry reactors. To guarantee that the photocatalyst stays in suspension in this system, turbulence is needed. But after usage, it is quite challenging to remove TiO2 from the liquid phase. According to Amir *et al.* (2017), meeting these standards also results in a significant increase in the energy used during the entire water treatment process. The research on the based photocatalytic oxidation process for organic pollutants and petroleum wastewater (produced water) treatment considered in this review is summaries in Tables 2.

**Table 2.** A summary of the uses of suspended TiO2 powder in photocatalytic treatment of oil and gas wastewater.

| Reference | Catalyst | Light source | Reactor | Degraded material | Notes |
|---|---|---|---|---|---|
| Natarajan *et al.* (2011) | $TiO_2$ (free) Powder Suspended | UV-LED λ=390–410 nm | 125 ml glass beaker and 5 UV-LED on acrylic sheet in circular path. | Rhodamine B dye (RhB) | 95% RhB degradation for 6 h |
| Qi *et al.* (2011) | $TiO_2$ (free) Powder | UV light | Annular reactor | Organic pollutants | CFD reactor simulation |
| Sarasidis *et al.* (2011) | $TiO_2$ (free) Powder Suspended | Three blue light bulbs λ=365nm | Photocatalytic reactor with ultrafiltration | Sodium alginate polysaccharides | 75% max. total organic carbon (TOC) removal |
| Jamali *et al.* (2013) | $TiO_2$ (free) Powder Suspended | UV LEDs 375 nm | Mini cylindrical vessel | Phenol | 87% Phenol degradation |
| (Boyjoo *et al.* 2014) | $TiO_2$/P25 suspension | with 2 or 4 artificial UV lamps | Annular reactor with catalyst suspension | Organic pollutants | CFD Increase in reaction rate 56% and 123% when using 2 and 4 lamps |
| (Dominguez *et al.* 2015) | $TiO_2$ (Free) powder Suspended | LED 375 nm In 10 strips and 18 units (180 LEDs) | A glass reaction vessel fitted inside PVC cylinder. | Dodecyl benzene sulfonate DBS Surfactants | 50% DBS degradation for 3 h |
| (Sarasidis *et al.* 2014) | $TiO_2$ (free) powder Suspended | Four black light bulbs, encased in acrylic containers | continuous membrane reactor, with hybrid catalysis | Diclofenac drug (DCF) | 96% DCF degradation |
| (Casado, Timmers, *et al.* 2017) | $TiO_2$ (free) powder Suspended | UV-LED 365 nm and UV black light fluorescent lamp 365–370 nm. | Two reactors, optically differential photoreactor annular lab. scale reactor | Methanol | CFD Kinetics of Oxidation methanol to formaldehyde |
| (B. Liu *et al.* 2016) | $TiO_2$ (free) powder Suspended | UV mercury lamp peak at 254 nm | Cylindrical glass jar covered by a quartz cap and sealed with a (PTFE) o-ring | Produced Water Polycyclic Aromatic Hydrocarbons (PAHs) | PAHs degradation was strongly restricted by the organic composition in OPW |
| (Turolla *et al.* 2016) | $TiO_2$/P25 powder Suspended | UV 254-355 nm | Annular reactor with suspension | Oxalic acid (OXA) | 90% OXA degradation |
| (Casado, Marugán, *et al.* 2017) | $TiO_2$/P25 powder Suspended | UV-LED 365 nm | Annular reactor with Suspension catalyst | Cinnamic acid (CA) | 80%, 90% CA degradation for 50, 100 mg/l CA for 1 h |
| (Casado *et al.* 2019) | $TiO_2$/P25 powder Suspended | solar simulator xenon lamp or Natural sunlight | Based on a tubular reactor and a compound parabolic collector, the solar reactor | Methanol | Oxidation of methanol to formaldehyde |
| (Silva *et al.* 2019) | $TiO_2$ (free) powder Suspended | UV lamps (253.7 nm) | glass beaker (500 ml) illuminated from the top | Phenolic in sea water and Produced Water (PW) | 99% for phenol elimination, no significant salt concentration |

### *2.2. Immobilization of Tio2 photocatalytic oxidation process*

Immobilized $TiO_2$ refers to the adhesion of titanium dioxide onto a support material, such as glass, silica, zeolites, or other porous materials the immobilization process usually enhances the practical application of TiO2 in photocatalysis, offering advantages such as easy recovery and reuse of the catalyst. According to several studies (Srikanth *et al.* 2017), using the photocatalyst supported (immobilized) by various materials in various reactor configurations has proven to be a good strategy to get around these challenges in recent years. As a catalyst in aqueous matrices, $TiO_2$ can be immobilized on a variety of inert support materials for use in fixed-film and fixed-bed reactors, or it can be used in a slurry reactor (Manassero *et al.* 2017). Additional significant technical problems include separating photocatalytic nanoparticles after water treatment and integrating them into workable reactor systems (Muritala *et al.* 2020). Before heterogeneous photocatalytic technology can be applied in industrial processes, it is necessary to develop nanoparticle

immobilization strategies that offer both a high photocatalytic activity and an affordable solid-liquid separation (Persico *et al.* 2015) ble 3. The general steps of immobilization strategy involve the following steps:

1. Selection of the suitable support material like glass, silica, metal oxide, etc. The slection method usually depends on the the intended application as well as the compatibility between the $TiO_2$ and the support material.
2. Ensuring that the selected material surface is clean and with no contamination. In most cases, it is important to enhance the adhesion of $TiO_2$. This is done by activation the surface of the support material either by cleaning, acid washing, or surface functionalization.
3. Preparing $TiO_2$ suspension through dispersing the $TiO_2$ powder in a suitable solvent.
4. Employing an immobilization process and it can be doen in several techniques involving the following:
5. So-gel process in which that a sol-gel solution of $TiO_2$ was prepared and applied onto the prepared surface support and dried to form the immobilized $TiO_2$ layer.
6. Dip-Coating in which that the support material submerged into $TiO_2$ suspension to allow the adsorption and then dried.
7. Chemical Bonding in which a chemical reaction occurred to create a chemical bond between $TiO_2$ and the support material.
8. Finaly, Heat treatment or calcination, in this step the coated support material is subjected to heat in furnace to remove any residual solvents and transfer the coated $TiO_2$ into stable and crystalline form.

An overview of prior studies employing the immobilized $TiO_2$ photocatalytic system are provided in Table3.

**Table 3.** Studies employing the immobilized TiO2 photocatalytic system.

| Reference | Catalyst | Light source | Reactor | Degraded material | Notes |
|---|---|---|---|---|---|
| (Duran *et al.* 2011) | Immobilized $TiO_2$ surface | UV 165-207 mm | $TiO_2$ surface immobilized on an annular reactor | Benzoic acid and 2,4-Dichlorophenoxy acetic acid | first order rate constant of 0.025 $min^{-1}$ |
| (Sampaio *et al.* 2013) | $TiO_2$-coated glass raschig rings | Simulated solar light irradiation | A glass cylindrical reactor packed with $TiO_2$-coated rings | Phenol | 90% Phenol degradation lose activity when reused |
| (Miranda-García *et al.* 2014) | Immobilized $TiO_2$ on glass spheres | UV range 290–800 nm (9% corresponds to UV radiation in the 290–400 nm range) | a pilot compound collector (CPC) solar plant | Multi contaminants | Regeneration treatments |
| El Yadini *et al.* (2014) | Immobilized $TiO_2$ on Borosilicate glass plates | UV 350- 400 nm peak 370 nm | Stirred tank reactor | Insecticide Fenamiphos | Degradation rate constants k=0.0183 $min^{-1}$ |
| Wang *et al.* (2015) | Immobilized $TiO_2$ on Diatomite | UV 250W Hg lamp. | Mini reactor 100 ml | Rhodamine B (RhB) | 90% RhB degradation for 1 h |
| (Barton *et al.* 2016) | $TiO_2$-coated glass sheets and optical fibers | UV mercury lamp 30 $W/m^2$ | Reactor glass beaker with side and top light source | Methylene blue (MB) and methyl orange (MO) | 1st order rate constant of about 1.55 $min^{-1}$ $g^{-1}$ |
| (Maculan *et al.* 2016) | Immobilized $TiO_2$ on metal plate coated with polyurethane resin and the catalyst. | UVsolar | Flat plate reactor | Dairy effluent | Reductions in COD (66.5%) and BOD (66.1%). |
| (Ramasundaram *et al.* 2016) | Immobilized $TiO_2$ on PVDF (poly vinylidene fluoride) coated Steel mesh (SM) | UV six blacklight blue lamps 350–400 nm | SM- $TiO_2$ was hung inside a 60-mL quartz reactor | Methylene Blue MB, methyl orange MO, reactive blue 4, sulfamethoxazole, and microcystin-LR | Degradation rate constants of 0.0251, 0.0368, 0.0164, 0.0568, and 0.0725 $min^{-1}$, respectively |
| Wang *et al.* (2016) | $TiO_2$ Supported Silica nanosheets composite | Visible light irradiation ≥400 nm | Continuous small container supported catalyst sheet | Phenol | 90% phenol degradation for 10 h |
| (Rokhmat *et al.* 2017) | $TiO_2$ nanoparticles coated on plastic granules | Sunlight irradiation wavelength longer than 300 nm | Hollow rectangular reactor with transparent glass | Methylene blue (MB) | 96.54% MB Degrading for 48 h |

| | | | | | |
|---|---|---|---|---|---|
| | | | at the top and a mirror at the bottom | | |
| (Cunha *et al.* 2018) | $TiO_2$ immobilized on glass spheres | UV-Vis's irradiation simulated the solar spectrum | Compound Parabolic Concentrator (CPC) reactor | Methylene blue (MB) | >96% MB degradation for 90 min |
| (Sraw *et al.* 2018) | $TiO_2$ immobilized clay beads | UV $\lambda_{max}$ 365 nm | Fixed bed recirculation catalyst immobilized clay beads | Pesticide Monocrotophos (MCP) | MCP degradation 78.57% |
| (Tugaoen *et al.* 2018) | $TiO_2$ coated optical fibers | UV- LED lamp 365 nm connected individual fiber bundle of fibers | PVC cylinder magnetic stirring optical fiber bundles at center | Para-chlorobenzoic acid (pCBA) | TiO2 coated optical fiber bundles enhanced pollutant removal |
| (Urkasame *et al.* 2018) | $TiO_2$– $SiO_2$ monolithic straight macropores (microhoney-combs) | UV- LED | Packed bed ground catalyst | Methylene blue (MB) | The conversion of MB reached a maximum at a calcination temperature of 600 °C. |
| (Cerrato *et al.* 2019) | Deposited micro- $TiO_2$ on glass Raschig rings | UV light | Packed column with coated glass Raschig rings | Ibuprofen (IBP) | Degraded 87 % of IBP in 6 h |
| Espindola *et al.* (2019) | $TiO_2$-P25 immobilized | UVA lamps λmax=365nm | Photocatalytic membrane reactor immobilized catalyst | Oxytetracycline (OTC) | Lower efficiency but stable permeate flux |
| Sacco *et al.* (2019) | structured N-doped $TiO_2$ supported on polystyrene (PS) spheres | visible light-emitting diodes (LEDs) | packed bed | Methylene Blue (MB) | almost complete decolorization achieved after 2 h |
| (Satuf *et al.* 2019) | immobilized $TiO_2$ surface | UV max 365 nm | Microfluidic reactor with catalyst films | Clofibric acid (CA) | 50% CA degradation for 8 h |
| (Pestana *et al.* 2020) | $TiO_2$ pelletized | UV | Packed bed continuous flow reactor | Microcystins (MC) | 51% MC degradation was observed. |
| Zhang *et al.* (2020) | $TiO_2$-coated glass beads | Xe-lamp | Capillary micro photoreactor packed bed | Methylene blue (MB) | |

### *2.3. Fe doped $TiO_2$ powder suspension photocatalytic process*

Fe-doped $TiO_2$ powder is titanium dioxide powder that has been loaded with iron (Fe). The dopping process is usually used to introduce specific properties enhancing the performance of various applications. This process includes integrating a certain number of iron ions into the $TiO_2$ crystal lattice. The dopping process are done through the following steps

1. Preparing the chemical materials involving titanium dioxide ($TiO_2$) powder, iron precursor (e.g., iron chloride, iron nitrate), solvent (e.g., water or organic solvent), reducing agent (if applicable), and surfactants or stabilizers
2. Dissolving the iron precursor with a suitable solvent to form a solution, after mixing that solution with titanium oxide powder. The doping level is determined by the used ratio of iron to titanium.
3. Mixing the prepared to ensure uniform distribution of the iron precursor.
4. Adjusting the pH level of the solution to control the doping efficiency.
5. Evaporating the solvent to get the dried powder
6. Heat treatment or calcination the dried powder in a furnace in a temperature range 400-800$^{o}$C. This step helped in crystalline the material and diffusing the iron ions into the $TiO_2$ lattice.

$TiO_2$ doped with Fe enhances the electrochemical and photochemical activities (Chatrnoor *et al.* 2023; Heda *et al.* 2023). The research on the Fe-doped $TiO_2$ powder solution photocatalytic process system utilized for the treatment is listed in Table 4.

$TiO_2$-based photocatalysts are commonly used to treat organic pollutants and petroleum industry wastewater. Wet impregnation technique (Realpe *et al.* 2016), reactive radio frequency sputtering (Nair *et al.* 2014), sol-gel (Komaraiah *et al.* 2019), mechanical alloying(Ranjit and Viswanathan 1997), co-precipitation(Z. Zhang *et al.* 1998), hydrothermal (Shi *et al.* 2018), microwave approach (Aba-Guevara *et al.* 2017), controlled hydrolysis (Dholam *et al.* 2009), RF plasma-enhanced chemical vapor deposition (Voleský 2015), and reactive magnetron sputtering are some of the methods that have been reported for doping Fe into $TiO_2$ structure. By drawing contaminants closer to the catalysts' active sites, immobilizing photocatalysts in the right kind of adsorptive material would make it easier to recover the catalysts and promote photodegradation (Shi *et a*l. 2020). Furthermore, for applications where the irradiation source is sunshine, buoyant immobilization material is extremely desirable. Thus, new supporting materials with high catalyst adherence, super adsorption capability, and tunable buoyancy-to-suspension interconversion are required for a variety of photocatalysis applications (Sboui *et al.* 2017). Table 4 illustrates the researcher's used Fe-doped $TiO_2$ powder in photocatalytic process.

**Table 4.** Studies on the photocatalytic process using Fe-doped $TiO_2$ powder suspension.

| Reference | Catalyst | Light source | Reactor | Degraded material | Notes |
|---|---|---|---|---|---|
| (George *et al.* 2011) | $TiO_2$ pure and Fe-Doped $TiO_2$ Nanoparticles | UV Xenon arc lamp with a light filter that transmits light in the range 350-450 nm | Well plates | N-acetyl-L tryptophanamide (NATA). | The rate of NATA oxidation increased with Fe content in TiO2 |
| (Ganesh *et al.* 2012) | Fe-doped $TiO_2$ powder | UV-Vis three wavelength ranges 400–475 nm, 475–550 nm and 800–1100 nm with three λmax peaks at t 433 nm, 512 nm and 900 nm | 75 mm tall by 150 mm wide glass dish | Methylene blue (MB) | 90% MB degradation, at 0.1 wt% Fe-doped TiO2 |
| Zhang and Zhu, (2012) | Fe-doped $TiO_2$ immobilized on polyamide fabric | sunlight and UV 254 nm light | fabric sample 5.0×6.5 cm was dipped into 50 ml of MB solution container | Methylene blue MB | 95% MB decolorization for sunlight at 2.5 h, and for UV at 6 h |
| Mwangi *et al.* (2013) | Fe (III)-doped $TiO_2$ immobilized on sintered glass | UV–Vis | Lab stirred Continuous circulation beaker with aeration. | Dissolved organic carbon (DOC) Starch solution | Fe-doped $TiO_2$ was activated using natural light |
| (Si *et al.* 2015) | Fe-doped $TiO_2$ catalyst | UV | Fluidized bed | Alizarin Green (AG) | AG Degradation rate constants 0.017 $min^{-1}$ |
| (Sood *et al.* 2015) | Fe-doped $TiO_2$ nanoparticles | Philips CFL bulb visible light 400 nm to 520 nm | Double walled batch photo reactor | Para-nitrophenol (PNP) | 92% maximum degradation in 5 h with Fe3+ 0.05 mol% |
| (Moradi *et al.* 2016) | Fe-doped $TiO_2$ nanoparticles | Visible light | Glass beaker under stirring. | Reactive red 198 (RR 198) | 40% RR198 decolorization for 5 h with 1 wt% Fe doped TiO2 |
| (Ali *et al.* 2017) | Fe-doped $TiO_2$ nanoparticles | Visible light | Pyrex glass well reactor with a magnetic stirring, water circulating jacket and a window for molecular oxygen supply | methylene blue (MB) | 75% MB removal at 3% Fe-doped TiO2 after 90 min |
| Foura *et al.* (2017) | Fe-Doped $TiO_2$ Supported on HY Zeolite | UV light at 254 nm | film flow Plexiglass rectangular workable area photocatalyst nanoparticles | Methylene blue (MB) | MB removal (>98%) was achieved after 1 h |

| | | | | | |
|---|---|---|---|---|---|
| | | | immobilized on the glass plate) | | |
| (Bansal & Verma 2018) | Fe-$TiO_2$ composite in free granules form | Sunlight | Non-concentrating solar recirculating fixed-bed reactor | Pentoxifylline (PEN) drug | 93% PEN removal after 4 h |
| Kaur *et al.* (2018) | Fe-Doped $TiO_2$ immobilized on clay beads | sunlight | Flat Plate | Carbendazim CBZ | Degradation 93% ± 4.65 for after 6 h |
| (El Mragui *et al.* 2019) | Pure $TiO_2$ Fe-doped $TiO_2$ Co-doped $TiO_2$ nanoparticles | UV-Vis | Pyrex cylindrical beaker 250 ml | Carbamazepine (CBZ) | CBZ removal With UV Fe/$TiO_2$> $TiO_2$ $TiO_2$>Co/ $TiO_2$ With Vis light Fe/$TiO_2$> Co/ $TiO_2$ Co/ $TiO_2$> $TiO_2$ |
| (Ghorbanpour & Feizi 2019) | Fe-doped $TiO_2$ | visible light | Rectangular photoreactor 50x50x50 cm made of MDF. | Methyl orange (MO) | The maximum degradation 69% at the Fe doping content of 0.5 wt%. |
| (Khan *et al.* 2019) | Fe-doped $TiO_2$ nanoparticles | Xenon lamp visible light (λ=400 nm) | stirred cylindrical vessel | methylene blue (MB) | 95% MB removal at 10% Fe-doped TiO2 after 3 h |
| (Liang *et al.* 2019) | Fe-doped $TiO_2$ powder | UV mercury lamp 365 nm and fluorescent lamp | 10 mL solution treating cell | Methyl orange (MO) | MO degradation 50% for visible 80% for UV at 0.3 mol% $Fe^{+3}$ |
| (Ahmed 2020) | Fe- $TiO_2$ crystals immobilized on fiberglass | LED 395-405 nm | Glass cylinder rectangular bar at center holds 12 LEDs, 3 on each to cover a 360-degree | Phenol | Degradation 85% after 90 min |
| Wang *et al.* (2021) | Fe-doped $TiO_2$ powder | mercury lamp λ=365 nm and visible fluorescent lamp | slurry container (25-50 ml) | Methyl orange (MO) | Degradation 1327.5 µg/g for UV light and 103.9 µg/g for visible light after 2 h |
| (Mancuso *et al.* 2021) | Fe-doped $TiO_2$ powder | A strip of visible-LEDs was positioned around the external body of the photoreactor | Pyrex cylindrical batch photoreactor D = 2.6 cm L = 41 cm V= 200 ml | AO7 dye total organic carbon (TOC) Phenol | 90% AO7 dye discoloration 40% TOC removal after 3 h |
| Ellouzi *et al.* (2022) | Fe-doped $TiO_2$ | hydrogen lamp Vis-L resource | A rectangular glass reactor filled with cold water. 125 mL quartz tube, installed inside the reactor. | Azo dye methyl orange (MO) | 4.2 times higher efficiency compared to pure $TiO_2$ |
| Matias *et al.* (2022) | Fe-Doped $TiO_2$ impregnated on porous polymeric platforms | LED solar simulator | Small magnetic agitation beaker | Rhodamine B (RhB) | Degradation 85% after 3.5 h |

## 3. Light source

Effective photocatalysts operate in the ultraviolet (UV) region of the light spectrum, which is expensive and energy consuming. To maximize efficiency, a wavelength in the ultraviolet region (<400 nm) is used for $TiO_2$-based photocatalyst activation (Oliveira *et al.* 2022). Figure 3 shows the light solar energy distribution received by the Earth. The amount of UV light that enters the atmosphere is minimal (approximately 5% of solar light). Visible light (vis) and infrared light (IR) make up the majority of the solar energy that the Earth receives (Barzagan 2022).

For the photocatalysis process, light sources are divided into either UV light with a wavelength range of 190-400 nm or visible light with a wavelength range of 400-780 nm.

Additionally, two light source types are employed: conventional lamps and light emitting diode (LED) lamps. Instead of UV lamps, two main types of LEDs—visible LEDs and UV LEDs—have been used for photochemical applications. For the purpose of researching the photocatalytic degradation of bisphenol, visible LED and carbon/nitrogen-doped $TiO_2$ were used leading to good results (Chen *et al.* 2005; Wang and Ku 2006; Chen and Dionysiou 2005; Wang and Lim 2010; Natarajan *et al.* 2011; Jamali *et al.* 2013).

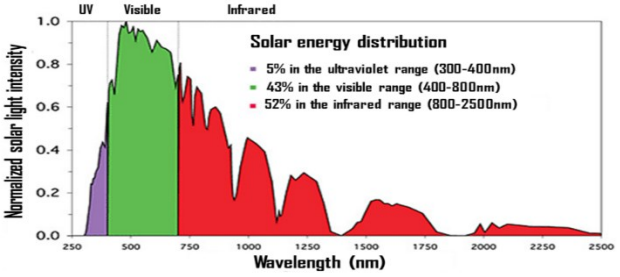


**Figure 3.** Light solar energy distribution received by the Earth (Barzagan 2022)

An LED is a semiconductor that emits light in a narrow spectrum, with different wavelengths (i.e., infrared, visible, or near ultraviolet) depending on the composition and condition of the semiconducting materials. LED output is directed and linearly correlated to the current flowing through its active region. In addition, LEDs are more cost-effective than traditional ultraviolet sources due to their small size and relatively long lifespan (greater than 50,000 h). Most UV curing, disinfection, sensing, and photocatalysis applications have traditionally employed conventional UV sources. However, LEDs have recently been recognized as an alternative to conventional ultraviolet irradiation sources; additionally, solar light can be utilized alongside LEDs for such applications (Jo & Tayade 2014).

Compared to traditional ultraviolet light irradiation sources, UV-LED technology possesses a number of benefits. These light sources are more energy-efficient and durable, and they have longer lifespans, while avoiding the mercury pollution issue with UV-A black lights and UV-C germicidal lamps. As a result of the homogeneity of the light dispersion found in slurry photoreactors, the reaction rates obtained from photocatalytic processes may be incorrectly analyzed. For catalysts immobilized on a surface, the creation of an effective photocatalytic reactor requires the simultaneous optimization of the light dispersion and the area occupied by the photocatalytic particles (Casado *et al.* 2017b).

## 4. Photocatalytic reactors

Photocatalytic reactor is the device at which the chemical reaction is facilitated through the use of photocatalysts. Several photocatalytic water treatments reactors have been created and tested during the previous 20 years. They can be categorized in several ways depending on their design and the operation conditions. According to their operating condition they can be classified as slurry photoreactor or immobilized photoreactor. As shown before, photocatalysts can be categorized by (1) form into powder (i.e., nano- or micro-sized particles) and (2) either suspended or immobilized (fixed), in which the catalyst is applied in a film on the wall surface of the reactor and on the supported particles or by pelletizing the powder to a large particle size (P. Liu *et al.* 2009; J. Liu *et al.* 2009). In comparison to suspended photocatalysts, supported photocatalysts have the benefit of not requiring a subsequent filtration step. But suspended photocatalysts often have a higher specific surface area than supported ones, which results in better degrading properties. Tables 5 show the advantages and disadvantages of slurry-type (suspended) and immobilized (fixed) photoreactors (Srikanth *et al.* 2017).

**Table 5.** Advantages and disadvantages of slurry-type and immobilized photoreactors (Srikanth *et al.* 2017).

| Slurry photoreactors | Immobilized photoreactors |
|---|---|
| Advantages<br>• The catalysts are dispersed uniformly.<br>• Greater illumination of the photocatalytic surface area in relation to the reactor volume<br>• Significantly reduced catalyst fouling effects due to the reactor's continual addition and removal of catalyst.<br>• A more effective suspension-based particle mixing.<br>• Lessened reactor-wide pressure drops.<br>• There are seldom any mass transfer restrictions. | Advantages<br>• Improvement in the removal of organic material from the aqueous phase while applying immobilizing agents with adsorptive qualities.<br>• Can offer continuous operation of the reactor.<br>• Can offer continuous operation of the reactor.<br>• It is quite simple to separate the catalyst from the final treated effluent stream. |
| Disadvantages<br>• Requires laborious and expensive post-treatment filtration procedures for the recovery of photocatalyst from the treated wastewater effluent streams.<br>• When there is a higher catalyst loading, suspended catalysts have a tendency to scatter light, slowing down photocatalytic activities.<br>• Catalytic particle aggregate, especially at greater concentrations. | Disadvantages<br>• The potential for catalyst washout and deactivation.<br>• Less photon accessibility to the catalyst.<br>• Considerable external mass transfer restrictions when the pollutant to be treated is flowing at low rates.<br>• With an increase in catalyst film thickness, internal mass transfer may play a dominant role by restricting the utilization of the supported photocatalyst, which is due to an increase in the diffusion path length of the reactant from the bulk to the catalyst surface. |

**Table 6.** Typical photocatalytic reactors (Cassano and Alfano 2000).

| Systems type | Reactor | Remark |
|---|---|---|
| Liquid-solid systems | Well-stirred slurries | Most commonly used as photocatalytic reactors |
| | Fluidized beds | Less widely used as photocatalytic reactors |
| | Packed beds | Less widely used as photocatalytic reactors |
| | Catalytic walls | Include membrane and fiber optic reactors, and Include membrane and fiber optic reactors. |
| Gas-liquid-solid systems | Trickle beds | Less widely used as photocatalytic reactors |
| | Packed bubble columns | |
| | Well-stirred slurries | |
| | Bubble column slurries | |
| | Fluidized beds | |
| | Moving beds | |

Cassano and Alfano (2000) have classified reactors for photocatalytic processes for wastewater treatments according to their contact phases, as shown in Table 6.

Depending on the design of the photocatalytic reactor, (Braham & Harris 2009) describe eight types of photocatalytic reactors, as follows:

1. Slurry, Fixed and Fluidized Bed Photoreactors
2. Parabolic Trough Reactors (PTR)
3. Compound Parabolic Collectors
4. Inclined Plate Collectors
5. Double-Skin Sheet Photoreactor
6. Rotating Disk Reactors
7. Water Bell Reactors
8. Optical Fiber Photoreactors

Ballari et al. (2019) discusses three types of reactors (i.e., slurry reactors, wall reactors, and fixed-bed reactors), classified according to geometry, modeling, and design purposes. In the cases of simpler geometries, such as continuous annular or flat-plate wall reactors, the design equations are essentially the same. Figure 4 shows the three types of photocatalytic reactors for wastewater treatment that employ artificial light: slurry reactor, packed-bed reactor, and fluidized-bed reactor.

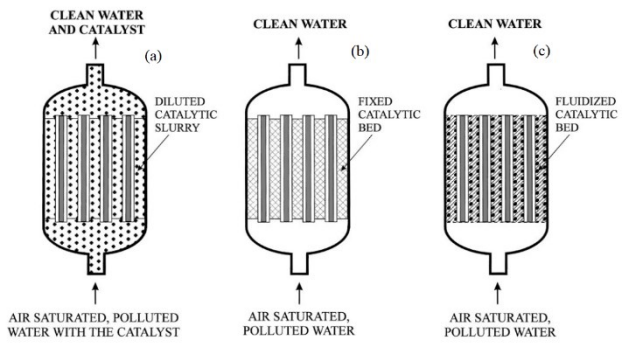


**Figure 4.** Photocatalytic reactors for wastewater that employ artificial light: (a) slurry reactor, (b) packed-bed reactor, and (c) fluidized-bed reactor (Cassano and Alfano 2000).

In slurry reactors, photocatalysts are suspended as tiny powders or nanoparticles in liquid media. Photocatalyst slurries have a greater surface area, providing a significant benefit. The cost of separating nanometer catalyst particles is a significant barrier to commercializing this technology. The light absorption in slurry systems cannot be separated from scattering, making kinetic analysis problematic. An alternate option involves attaching the catalyst to a clear stationary support that the tainted water travels through. This method can effectively illuminate all photocatalysts installed in the reactor. An early study on slurry reactor had been done o the mineralization of chloroform into chloride and $CO_2$. Kormann et al. found that while chloroform was completely dehalogenated, [$Cl^-$] increased over time (Kormann *et al.* 1991). Li Puma and Yue studied the degradation kinetics of both single and multi-component chlorophenols. The researchers investigated the combination of photocatalysis and photolysis using short, medium, and long wavelength ultraviolet light simultaneously (Li Puma G and Yue PL. 1999). A $TiO_2$ slurry reactor was used to evaluate the adsorption and photocatalytic degradation of Safira HEXL dye (Jone, *et al.* 2005). The researchers found that dye adsorption to the photocatalyst surface was crucial for effective degradation. The process was pH-dependent, with a faster breakdown rate found at low $TiO_2$ charge.

The study of the photocatalytic degradation of organic wastewater in a laboratory slurry photocatalytic reactor is similar to that used for the degradation of polycyclic aromatic hydrocarbons in produced water ((B. Liu *et al.* 2016), as shown in Figure 5.

The packed-bed reactors use a solid support, often a photocatalyst bed, to flow reactants. The photocatalyst is immobilized on a support structure, and reactants pass over or through the catalyst bed, which is exposed to light for reaction.

Nogueira and Jardim studied the photodegradation of methylene blue utilizing sun irradiation in a fixed bed reactor with TiO2 immobilized on a flat glass plate. The slope of the plate affects methylene blue

photodegradation due to two factors: fluid thickness and light intensity. The study indicated that 95.8% of the model compound deteriorated at a 22◦ slope and 89% at a 25◦ angle (Nogueira and Jardim 1996). Feitz et al. studied two fixed bed photocatalytic reactors: a packed bed reactor and a coated mesh reactor, utilizing solar illumination. The processing rate for 2 mg $L^{-1}$ phenol solutions was computed as 140 mg $m^{-2}$ $h^{-1}$ for the packed bed reactor and 20 mg $m^{-2}$ $h^{-1}$ for the coated mesh reactor. The coated mesh reactor showed decreased activity due to inadequate photocatalyst surface contact, low $TiO_2$ levels, and a small reactor-to-tank volume ratio. The packed bed unit demonstrated 40% lower photonic efficiencies than suspension systems while decomposing 100 $mg^{-1}$ dichloroacetic acid solutions. The authors suggested that this approach was highly successful (Feitz et al. 200). A tubular photocatalytic TiO2 coating produced via sol-gel was used by (Lin *et al.* 2003). They studied a reactor with recirculation mode and a batch photocatalytic reactor for the breakdown of methylene blue and phenol. The researchers suggest using the synthesized sol-gel film for water purification due to its excellent photocatalytic activity in decomposing organic molecules. I their work, a 180-minute photoreaction of phenanthrene resulted in 67.6% destruction and 40.1% conversion to $CO_2$.

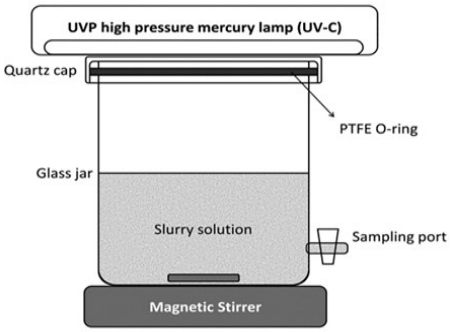


**Figure 5.** Laboratory slurry photocatalytic reactor (B. Liu *et al.* 2016).

The photocatalytic oxidation of a non-ionic surfactant was performed in a labyrinth flow reactor with an immobilized photocatalyst bed (Mozia *et al.* 2005). The study examined how flow rate affects the breakdown of non-ionic surfactants. The researchers found that photodegradation of the surfactant was most effective at a flow velocity of 11.98 $dm^3$ $h^{-1}$. The researchers further, investigated the remediation of Acid Red 18, an azo dye (Mozia *et al.* 2007). An immobilized Aeroxide Degussa P25 catalyst was used to study the photodegradation of Acid Red over longer reaction durations. Mineralization timeframes ranged from 35 to 60 hours based on flow rate, indicating that slower flow rates reduced system efficiency.

Fluidized bed reactors, like fixed-bed reactors, employ a solid support for their photocatalysts. However, in this scenario, the movement of gas or liquid reactants suspends and fluidizes the catalyst particles. This increases mass transfer and the effectiveness of the photocatalytic process.

Nelson *et al.* compared a fluidized TiO2 system for methanol oxidation to a packed bed reactor. The study found that fluidization led to quicker photocatalytic breakdown rates compared to packed bed units. The fluidized reactor produced CO2 at a rate of $2.0 \times 10^{-7}$ mol $cm^{-3}$ $min^{-1}$, while the packed bed reactor produced only $1.0 \times 10^{-7}$ mol $cm^{-3}$ $min^{-1}$. Static mixing and vibration were shown to diminish photocatalyst separation rates with Degussa P25, but not with $TiO_2$ -$Al_2O_3$ (Nelson et al. 2007) Overall, $TiO_2$-$Al_2O_3$ was shown to be an effective photocatalyst, consistent with Paz's results (Paz 2010).

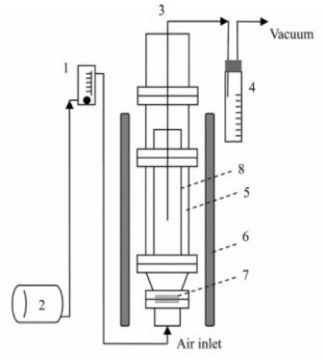


**Figure 6.** A small-scale, gas-liquid-solid, three-phase, fluidized-bed photoreactor: (1) flow controller, (2) compressor, (3) sampling tube, (4) sampling tank, (5) Pyrex® glass cylindrical vessel, (6) black light lamps, (7) gas distributor, and (8) draft tube (Matsumura *et al.* 2007).

A small-scale, gas-liquid-solid, three-phase, fluidized-bed photoreactor is shown in Figure 6 (Matsumura *et al.* 2007).

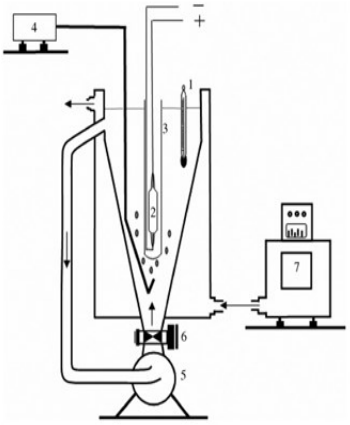


**Figure 7.** Conical-shaped circulating upflow reactor: (1) thermometer, (2) UV lamp, (3) quartz tube, (4) micro air compressor, (5) circulating pump, (6) valve, and (7) thermostat (Saien and Nejati 2007).

Tapered bubble columns (TBCs) are used for a range of processes, such as wastewater treatment, exothermic reactions, biofilm reactions, nuclear fuel particle coating, coal gasification, sulfide ores roasting, and food processing (Bandyopadhyay *et al.* 2011). TBCs are a specific type of bubble column reactor with a cross-sectional area that increases progressively down the vertical axis. The use of a higher superficial gas velocity ensures the suspension of heavier particles (with higher terminal particle settling velocities) at the bottom, while a lower superficial gas velocity prevents the entrainment of lighter particles (with lower terminal particle settling velocities) at the top. Therefore, tapered columns allow for extensive particle mixing and a wider range of particle size distributions

compared to traditional cylindrical columns (K. Zhang *et al.* 2003).

Saien and Soleymani (2007) used an annular and conic body shape circulating upflow reactor with a UV lamp at the center with no dead zone, as shown in Figure 7. About 50% removal of the chemical oxygen demand (COD) was obtained and 97% of dye degradation was achieved at the following operating conditions: 40 mg/l catalyst, 6.2 pH, 45ºC, and 2 h irradiation.

## 5. Conclusions

This review shows how photocatalytic approaches have considerably improved the treatment of severely polluted industrial wastewater. There is evidence that TiO2-based photocatalysts decompose organic contaminants more efficiently than other photocatalytic systems for wastewater treatment. The photocatalyst's physicochemical properties are influenced by the synthesis technique, chemical composition, and technological aspects.

Organic contaminants in wastewater can be considerably decreased by upgrading photoreactors, which convert pollutants to $CO_2$ and $H_2O$ using photocatalysts. Although there are other types of catalysts, $TiO_2$ is one of the most commonly employed in the process. Pure $TiO_2$ absorbs relatively little sunlight, and photocatalysis needs UV radiation. Doping with metal ions such as Fe enhances electrochemical and photochemical activities, introducing new energy levels into the bandgap and decreasing the gap to the visible range.

Improved photocatalytic performance can be achieved by investigating the synergistic effects of various operating conditions. Despite major recent advances, decreasing efficiency and reutilization remain poor, making them unsuitable for use in practical applications.

The effectiveness of photocatalysis is heavily impacted by the operating parameters and reactor designs employed. In a photocatalytic reactor, elements such as degradation concentration, pH, temperature, charged nature of the pollutant, reactor, light source (lamp), and catalyst are all critical to achieve maximum efficiency. As a result, while developing and manufacturing photocatalysts for the treatment of organic pollutants, all critical parameters must be carefully examined.

The choice of a specific photocatalytic reactor type depends on the nature of the reaction, desired product, and other process parameters. Each type has its advantages and limitations, and researchers and engineers select the most suitable design based on the specific requirements of their application.

Immobilization for recycling, photocatalyst optimization, and reactor design to increase the separation efficiency are all crucial components needed to advance the development of innovative photocatalytic systems.

## 6. References

Abdullah R.R., Shabeeb K.M., Alzubaydi A.B., Figoli A., Criscuoli A., Drioli E. and Alsalhy Q. (2022). Characterization of the Efficiency of Photo-Catalytic Ultrafiltation PES Membrane Modified with Tungsten Oxide in the Removal of Tinzaparin Sodium. *Eng. Technol. J*, *40*, 1–10.

Ahmad R., Ahmad Z., Khan A.U., Mastoi N.R., Aslam M. and Kim J. (2016). Photocatalytic systems as an advanced environmental remediation: Recent developments, limitations and new avenues for applications. *Journal of Environmental Chemical Engineering*, **4(4)**, 4143–4164.

Ahmed F. (2020). *Synthesis and characterization of Fe-doped TiO2 on fiberglass cloth for the wastewater treatment reactor*.

Al-Nuaim M.A., Alwasiti A.A. & Shnain Z.Y. (2023) The photocatalytic process in the treatment of polluted water. Chem. Pap. **77**, 677–701. https://doi.org/10.1007/s11696-022-02468-7.

Al-Nuaim M., Al-Wasiti A.A., Shnain Z.Y. and Al-Shalal A.K. (2022). The combined effect of bubble and photo catalysis technology in BTEX removal from produced water. *Bulletin of Chemical Reaction Engineering & Catalysis*, **17(3)**, 577–589.

Ali T., Tripathi P., Azam A., Raza W., Ahmed A.S., Ahmed A. and Muneer M. (2017). Photocatalytic performance of Fe-doped TiO2 nanoparticles under visible-light irradiation. *Materials Research Express*, **4(1)**, 15022.

Aljuboury D., Palaniandy P., Abdul Aziz H.B. and Feroz S. (2017). Treatment of petroleum wastewater by conventional and new technologies-A review. *Glob. Nest J*, **19(3)**, 439–452.

Ani I.J., Akpan U.G., Olutoye M.A. and Hameed B.H. (2018). Photocatalytic degradation of pollutants in petroleum refinery wastewater by TiO2-and ZnO-based photocatalysts: recent development. *Journal of Cleaner Production*, *205*, 930–954.

Ballari M. de los M., Satuf M.L. and Alfano O.M. (2020). Photocatalytic reactor modeling: application to advanced oxidation processes for chemical pollution abatement. *Heterogeneous Photocatalysis: Recent Advances*, 265–301.

Bandyopadhyay A. and Biswas M.N. (2011). Hydrodynamics of a tapered bubble column. *Chemical Engineering & Technology*, **34(2)**, 186–200.

Bansal P. and Verma A. (2018). In-situ dual effect studies using novel Fe-TiO2 composite for the pilot-plant degradation of pentoxifylline. *Chemical Engineering Journal*, *332*, 682–694.

Barton I., Matejec V. and Matousek J. (2016). Photocatalytic activity of nanostructured TiO2 coating on glass slides and optical fibers for methylene blue or methyl orange decomposition under different light excitation. *Journal of Photochemistry and Photobiology A: Chemistry*, *317*, 72–80.

Barzagan A. (2022). *Photocatalytic Water and Wastewater Treatment*. IWA Publishing.

Bettini L.G., Diamanti M.V., Sansotera M., Pedeferri M.P., Navarrini W. and Milani P. (2016). Immobilized TiO 2 nanoparticles produced by flame spray for photocatalytic water remediation. *Journal of Nanoparticle Research*, *18*, 1–10.

Boyjoo Y., Ang M. and Pareek V. (2014). CFD simulation of a pilot scale slurry photocatalytic reactor and design of multiple-lamp reactors. *Chemical Engineering Science*, *111*, 266–277.

Braham R.J. and Harris A.T. (2009). Review of major design and scale-up considerations for solar photocatalytic reactors. *Industrial & Engineering Chemistry Research*, **48(19)**, 8890–8905.

Casado C., Garcia-Gil A., van Grieken R. and Marugan J. (2019). Critical role of the light spectrum on the simulation of solar

photocatalytic reactors. *Applied Catalysis B: Environmental*, *252*, 1–9.

Casado C., Marugán J., Timmers R., Muñoz M. and van Grieken R. (2017). Comprehensive multiphysics modeling of photocatalytic processes by computational fluid dynamics based on intrinsic kinetic parameters determined in a differential photoreactor. *Chemical Engineering Journal*, *310*, 368–380.

Casado C., Timmers R., Sergejevs A., Clarke C.T., Allsopp D.W.E., Bowen C.R., Van Grieken R. and Marugán J. (2017). Design and validation of a LED-based high intensity photocatalytic reactor for quantifying activity measurements. *Chemical Engineering Journal*, *327*, 1043–1055.

Cassano A.E. and Alfano O.M. (2000). Reaction engineering of suspended solid heterogeneous photocatalytic reactors. *Catalysis Today*, **58(2–3)**, 167–197.

Cerrato G., Bianchi C.L., Galli F., Pirola C., Morandi S. and Capucci V. (2019). Micro-TiO2 coated glass surfaces safely abate drugs in surface water. *Journal of Hazardous Materials*, *363*, 328–334.

Chatrnoor S., Taghadossi A.H., Alem S.A.A., Taati-Asil F., Raissi B., Riahifar R. and Yaghmaee M.S. (n.d.). Synthesizing Fe-Doped Tio2 Nanoparticles by Anodic Dissolution Method and Preparing An Electrophoretic Deposited Layer. *Available at SSRN 4369392*.

Chen D., Cheng Y., Zhou N., Chen P., Wang Y., Li K., Huo S., Cheng P., Peng P. and Zhang R. (2020). Photocatalytic degradation of organic pollutants using TiO2-based photocatalysts: A review. *Journal of Cleaner Production*, *268*, 121725.

Chen D.H., Ye X. and Li K. (2005). Oxidation of PCE with a UV LED photocatalytic reactor. *Chemical Engineering & Technology: Industrial Chemistry-Plant Equipment-Process Engineering-Biotechnology*, **28(1)**, 95–97.

Chen X., Yang J. and Zhang J. (2004). Preparation and photocatalytic properties of Fe-doped TiO2 nanoparticles. *Journal of Central South University of Technology*, **11(2)**, 161–165.

Chen Y. and Dionysiou D.D. (2005). *High Performance TiO2 Photocatalytic Coatings and Reactors for the Purification, Disinfection and Recycle of Water in Space Applications*. SAE Technical Paper.

Chen Y. and Dionysiou D.D. (2007). A comparative study on physicochemical properties and photocatalytic behavior of macroporous TiO2-P25 composite films and macroporous TiO2 films coated on stainless steel substrate. *Applied Catalysis A: General*, **317(1)**, 129–137.

Corradi A.B., Bondioli F., Focher B., Ferrari A.M., Grippo C., Mariani E. and Villa C. (2005). Conventional and microwave-hydrothermal synthesis of TiO2 nanopowders. *Journal of the American Ceramic Society*, **88(9)**, 2639–2641.

Cunha D.L., Kuznetsov A., Achete C.A., da Hora Machado A.E. and Marques M. (2018). Immobilized TiO2 on glass spheres applied to heterogeneous photocatalysis: Photoactivity, leaching and regeneration process. *PeerJ*, *6*, e4464.

Devi L.G., Nithya P.M., Abraham C. and Kavitha R. (2017). Influence of surface metallic silver deposit and surface fluorination on the photocatalytic activity of rutile TiO2 for the degradation of crystal violet a cationic dye under UV light irradiation. *Materials Today Communications*, *10*, 1–13.

Diya'uddeen B.H., Daud W.M.A.W. and Aziz A.R.A. (2011). Treatment technologies for petroleum refinery effluents: A review. *Process Safety and Environmental Protection*, **89(2)**, 95–105.

Dominguez S., Ribao P., Rivero M.J. and Ortiz I. (2015). Influence of radiation and TiO2 concentration on the hydroxyl radicals generation in a photocatalytic LED reactor. Application to dodecylbenzenesulfonate degradation. *Applied Catalysis B: Environmental*, *178*, 165–169.

Drozd V.S., Zybina N.A., Abramova K.E., Parfenov M.Y., Kumar U., Valdés H., Smirniotis P.G. and Vorontsov A.V. (2019). Oxygen vacancies in nano-sized TiO2 anatase nanoparticles. *Solid State Ionics*, *339*, 115009.

Duran J.E., Mohseni M. and Taghipour F. (2011). Computational fluid dynamics modeling of immobilized photocatalytic reactors for water treatment. *AIChE Journal*, **57(7)**, 1860–1872.

El Mragui A., Logvina Y., Pinto da Silva L., Zegaoui O. and Esteves da Silva J.C.G. (2019). Synthesis of Fe-and Co-doped TiO2 with improved photocatalytic activity under visible irradiation toward carbamazepine degradation. *Materials*, **12(23)**, 3874.

El Yadini A., Saufi H., Dunlop P.S.M., Byrne J.A., El Azzouzi M. and El Hajjaji S. (2014). Supported TiO2 on borosilicate glass plates for efficient photocatalytic degradation of fenamiphos. *Journal of Catalysts*, *2014*.

Ellouzi I., Regraguy B., El Hajjaji S., Harir M., Schmitt-Kopplin P., Lachheb H. and Laânab L. (2022). Synthesis of Fe-doped TiO2 with improved photocatalytic properties under Vis-L irradiation. *Iranian Journal of Catalysis,* **12(3)**, 283–293.

Elmobarak W.F., Hameed B.H., Almomani F. and Abdullah A.Z. (2021). A review on the treatment of petroleum refinery wastewater using advanced oxidation processes. *Catalysts*, **11(7)**, 782.

Espindola J.C., Cristovao R.O., Mendes A., Boaventura R.A.R. and Vilar V.J.P. (2019). Photocatalytic membrane reactor performance towards oxytetracycline removal from synthetic and real matrices: Suspended vs immobilized TiO2-P25. *Chemical Engineering Journal*, *378*, 122114.

Feitz AJ, Boyden BH and Waite TD (2000), Evaluation of two solar pilot scale fixed-bed photocatalytic reactors. Water Res 34:3927–3932.

Foura G., Chouchou N., Soualah A., Kouachi K., Guidotti M. and Robert D. (2017). Fe-doped TiO2 supported on HY zeolite for solar photocatalytic treatment of dye pollutants. *Catalysts*, **7(11)**, 344.

Ganesh I., Kumar P.P., Gupta A.K., Sekhar P.S.C., Radha K., Padmanabham G. and Sundararajan G. (2012). Preparation and characterization of Fe-doped TiO 2 powders for solar light response and photocatalytic applications. *Processing and Application of Ceramics*, **6(1)**, 21–36.

George S., Pokhrel S., Ji Z., Henderson B.L., Xia T., Li L., Zink J.I., Nel A.E. and Mädler L. (2011). Role of Fe doping in tuning the band gap of TiO2 for the photo-oxidation-induced cytotoxicity paradigm. *Journal of the American Chemical Society*, **133(29)**, 11270–11278.

Ghorbanpour M. and Feizi A. (2019). Iron-doped TiO2 catalysts with photocatalytic activity. *Journal of Water and Environmental Nanotechnology*, **4(1)**, 60–66.

Gogate P.R. and Pandit A.B. (2004). A review of imperative technologies for wastewater treatment I: oxidation technologies at ambient conditions. *Advances in Environmental Research*, **8(3–4)**, 501–551.

Gotić M., Ivanda M., Sekulić A., Musić S., Popović S., Turković A. and Furić K. (1996). Microstructure of nanosized TiO2 obtained by sol-gel synthesis. *Materials Letters*, **28(1–3)**, 225–229.

Heda N.L., Kumar K., Sharma V., Ahuja U., Dalela S. and Ahuja B.L. (2023). Impact of Co doping on electronic response, momentum densities and localisation of d electrons of TiO2: Compton profiles and first-principles calculations. *Materials Today Communications*, *34*, 105144.

Ibhadon A.O. and Fitzpatrick P. (2013). Heterogeneous photocatalysis: recent advances and applications. *Catalysts*, **3(1)**, 189–218.

Jamali A., Vanraes R., Hanselaer P. and Van Gerven T. (2013). A batch LED reactor for the photocatalytic degradation of phenol. *Chemical Engineering and Processing: Process Intensification*, *71*, 43–50.

Jeon M.S., Yoon W.S., Joo H., Lee T.K. and Lee H. (2000). Preparation and characterization of a nano-sized Mo/Ti mixed photocatalyst. *Applied Surface Science*, **165(2–3)**, 209–216.

Jeon J, Kim S, Lim T and Lee D, (2005) Degradation of trichloroethylene by photocatalysis in an internally circulating slurry bubble column reactor. Chemosphere 60:1162–1168.

Jo W.-K. and Tayade R.J. (2014). New generation energy-efficient light source for photocatalysis: LEDs for environmental applications. *Industrial & Engineering Chemistry Research*, **53(6)**, 2073–2084.

Kaur A., Umar A. and Kansal S.K. (2016). Heterogeneous photocatalytic studies of analgesic and non-steroidal anti-inflammatory drugs. *Applied Catalysis A: General*, *510*, 134–155.

Kaur T., Sraw A., Wanchoo R.K. and Toor A.P. (2018). Solar assisted degradation of carbendazim in water using clay beads immobilized with TiO2 & Fe doped TiO2. *Solar Energy*, *162*, 45–56.

Khan M.A.M., Siwach R., Kumar S. and Alhazaa A.N. (2019). Role of Fe doping in tuning photocatalytic and photoelectrochemical properties of TiO2 for photodegradation of methylene blue. *Optics & Laser Technology*, *118*, 170–178.

Kim Sang-don (2000). Gas Holdup and Bubble Characteristics in Tapered Bubble Columns. *Korean Chemical Engineering Research (Hwahak Konghak)*, **38(6)**, 864–868.

Kormann C, Bahnemann DW and Hoffmann MR (1991), Photolysis of chloroform and other organic molecules in aqueous titanium dioxide suspensions. Environ Sci Technol 25:494–500.

Li Y., Chen J., Liu J., Ma M., Chen W. and Li L. (2010). Activated carbon supported TiO2-photocatalysis doped with Fe ions fo continuous treatment of dye wastewater in a dynamic reactor. *Journal of Environmental Sciences*, **22(8)**, 1290–1296.

Li Y., Ma Y., Li K., Chen S. and Yue D. (2022). Photocatalytic reactor as a bridge to Link the commercialization of photocatalyst in water and air purification. *Catalysts*, **12(7)**, 724.

Li Puma G and Yue PL (1999), Enhanced photocatalysis in a pilot laminar falling film slurry reactor. Ind Eng Chem Res 38:3246–3254.

Liang D., Liu S., Wang Z., Guo Y., Jiang W., Liu C., Wang H., Wang N., Ding W. and He M. (2019). Coprecipitation synthesis of N, Fe doped anatase TiO 2 nanoparticles and photocatalytic mechanism. *Journal of Materials Science: Materials in Electronics*, *30*, 12619–12629.

Lin HF and Valsaraj KT (2003) A titania thin film annular photocatalytic reactor for the degradation of polycyclic aromatic hydrocarbons in dilute water streams. J Hazard Mater 99:203–219.

Liu B., Chen B., Zhang B.Y., Jing L., Zhang H. and Lee K. (2016). Photocatalytic degradation of polycyclic aromatic hydrocarbons in offshore produced water: effects of water matrix. *Journal of Environmental Engineering*, **142(11)**, 4016054.

Liu J., Dong M., Zuo S. and Yu Y. (2009). Solvothermal preparation of TiO2/montmorillonite and photocatalytic activity. *Applied Clay Science*, **43(2)**, 156–159.

Maculan J.L., Luzza M., Pokrywiecki J.C., Dusmann E., Tonial I.B. and Pokrywiecki T.S. (2016). Aplicação de fotoirradiação solar para tratamento de efluentes de laticínios. *Tecnologia e Ambiente*, *22*.

Manassero A., Satuf M.L. and Alfano O.M. (2017). Photocatalytic degradation of an emerging pollutant by TiO 2-coated glass rings: a kinetic study. *Environmental Science and Pollution Research*, *24*, 6031–6039.

Mancuso A., Sacco O., Vaiano V., Bonelli B., Esposito S., Freyria F.S., Blangetti N. and Sannino D. (2021). Visible light-driven photocatalytic activity and kinetics of Fe-doped TiO2 prepared by a three-block copolymer templating approach. *Materials*, **14(11)**, 3105.

Manzoor M., Rafiq A., Ikram M., Nafees M. and Ali S. (2018). Structural, optical, and magnetic study of Ni-doped TiO 2 nanoparticles synthesized by sol–gel method. *International Nano Letters*, *8*, 1–8.

Marami M.B., Farahmandjou M. and Khoshnevisan B. (2018). Sol–gel synthesis of Fe-doped TiO 2 nanocrystals. *Journal of Electronic Materials*, *47*, 3741–3748.

Matias M.L., Pimentel A., Reis-Machado A.S., Rodrigues J., Deuermeier J., Fortunato E., Martins R. and Nunes D. (2022). Enhanced Fe-TiO2 solar photocatalysts on porous platforms for water purification. *Nanomaterials*, **12(6)**, 1005.

Matsumura T., Noshiroya D., Tokumura M., Znad H.T. and Kawase Y. (2007). Simplified Model for the Hydrodynamics and Reaction Kinetics in a Gas− Liquid− Solid Three-Phase Fluidized-Bed Photocatalytic Reactor: Degradation of o-Cresol with Immobilized TiO2. *Industrial & Engineering Chemistry Research*, **46(8)**, 2637–2647.

Miranda-García N., Suárez S., Maldonado M.I., Malato S. and Sánchez B. (2014). Regeneration approaches for TiO2 immobilized photocatalyst used in the elimination of emerging contaminants in water. *Catalysis Today*, *230*, 27–34.

Moradi H., Eshaghi A., Hosseini S.R. and Ghani K. (2016). Fabrication of Fe-doped TiO2 nanoparticles and investigation of photocatalytic decolorization of reactive red 198 under visible light irradiation. *Ultrasonics Sonochemistry*, *32*, 314–319.

Mozia S, Tomaszewska M and Morawski AW (2005) Photocatalytic degradation of azo-dye Acid Red 18. Desalination 185:449–456.

Mozia S, Tomaszewska M and Morawski AW (2007) Photodegradation of azo dye Acid Red 18 in a quartz labyrinth flow reactor with immobilized TiO2 bed. Dyes Pigments 75:60–66.

Muritala I.K., Guban D., Roeb M. and Sattler C. (2020). High temperature production of hydrogen: Assessment of non-

renewable resources technologies and emerging trends. *International Journal of Hydrogen Energy*, **45(49)**, 26022–26035.

Mwangi I.W., Ngila J.C., Ndungu P., Msagati T.A.M. and Kamau J.N. (2013). Immobilized Fe (III)-doped titanium dioxide for photodegradation of dissolved organic compounds in water. *Environmental Science and Pollution Research*, *20*, 6028–6038.

Nair P.B., Justinvictor V.B., Daniel G.P., Joy K., Ramakrishnan V., Kumar D.D. and Thomas P.V. (2014). Structural, optical, photoluminescence and photocatalytic investigations on Fe doped TiO2 thin films. *Thin Solid Films*, *550*, 121–127.

Natarajan T.S., Thomas M., Natarajan K., Bajaj H.C. and Tayade R.J. (2011). Study on UV-LED/TiO2 process for degradation of Rhodamine B dye. *Chemical Engineering Journal*, **169(1–3)**, 126–134.

Nelson RJ, Flakker CL and Muggli DS (2007). Photocatalytic oxidation of methanol using titania-based fluidized beds. Appl Catal B: Environ 69:189–195.

Nogueira RFP and Jardim WF (1996), TiO2-fixed-bed reactor for water decontamination using solarlight. SolarEnergy 56:471–477.

Oliveira T.P., Rodrigues S.F., Marques G.N., Viana Costa R.C., Garçone Lopes C.G., Aranas Jr C., Rojas A., Gomes Rangel J.H. and Oliveira M.M. (2022). Synthesis, characterization, and photocatalytic investigation of CuFe2O4 for the degradation of dyes under visible light. *Catalysts*, **12(6)**, 623.

Paz Y. (2010) Application of TiO2 photocatalysis for air treatment: patents' overview. Appl Catal B: Environ 99:448–460.

Peng Y.-H., Huang G.-F. and Huang W.-Q. (2012). Visible-light absorption and photocatalytic activity of Cr-doped TiO2 nanocrystal films. *Advanced Powder Technology*, **23(1)**, 8–12.

Persico F., Sansotera M., Bianchi C.L., Cavallotti C. and Navarrini W. (2015). Photocatalytic activity of TiO2-embedded fluorinated transparent coating for oxidation of hydrosoluble pollutants in turbid suspensions. *Applied Catalysis B: Environmental*, *170*, 83–89.

Pestana C.J., Hobson P., Robertson P.K.J., Lawton L.A. and Newcombe G. (2020). Removal of microcystins from a waste stabilisation lagoon: Evaluation of a packed-bed continuous flow TiO2 reactor. *Chemosphere*, *245*, 125575.

Pozzo R.L., Brandi R.J., Giombi J.L., Cassano A.E. and Baltanás M.A. (2006). Fluidized bed photoreactors using composites of titania CVD-coated onto quartz sand as photocatalyst: Assessment of photochemical efficiency. *Chemical Engineering Journal*, **118(3)**, 153–159.

Qi N., Zhang H., Jin B. and Zhang K. (2011). CFD modelling of hydrodynamics and degradation kinetics in an annular slurry photocatalytic reactor for wastewater treatment. *Chemical Engineering Journal*, **172(1)**, 84–95.

Ramasundaram S., Seid M.G., Choe J.W., Kim E.-J., Chung Y.C., Cho K., Lee C. and Hong S.W. (2016). Highly reusable TiO2 nanoparticle photocatalyst by direct immobilization on steel mesh via PVDF coating, electrospraying, and thermal fixation. *Chemical Engineering Journal*, *306*, 344–351.

Rokhmat M., Wibowo E., Murniati R. and Abdullah M. (2017). Novel solar photocatalytic reactor for wastewater treatment. *IOP Conference Series: Materials Science and Engineering*, **214(1)**, 12010.

Sacco O., Sannino D., Matarangolo M. and Vaiano V. (2019). Room temperature synthesis of V-doped TiO2 and its photocatalytic activity in the removal of caffeine under UV irradiation. *Materials*, **12(6)**, 911.

Sacco O., Sannino D. and Vaiano V. (2019). Packed bed photoreactor for the removal of water pollutants using visible light emitting diodes. *Applied Sciences*, **9(3)**, 472.

Sajda S. Alsaedi, Seba Saeed Mohammed, Alyaa Esam Mahdi, Zainab Y. Shnain, Hasan Sh. Majdi, Adnan A. AbdulRazak & Asawer A. Alwasiti (2024) Modeling spinel oxide based-photocatalytic degradation of organic pollutants from industrial wastewater, Chemical Engineering Communications, 211:4, 603-613, DOI: 10.1080/00986445.2023.2269526

Sampaio M.J., Silva C.G., Silva A.M.T., Vilar V.J.P., Boaventura R.A.R. and Faria J.L. (2013). Photocatalytic activity of TiO2-coated glass raschig rings on the degradation of phenolic derivatives under simulated solar light irradiation. *Chemical Engineering Journal*, *224*, 32–38.

Sarasidis V.C., Patsios S.I. and Karabelas A.J. (2011). A hybrid photocatalysis–ultrafiltration continuous process: The case of polysaccharide degradation. *Separation and Purification Technology*, **80(1)**, 73–80.

Sarasidis V.C., Plakas K.V, Patsios S.I. and Karabelas A.J. (2014). Investigation of diclofenac degradation in a continuous photo-catalytic membrane reactor. Influence of operating parameters. *Chemical Engineering Journal*, *239*, 299–311.

Satuf M.L., Macagno J., Manassero A., Bernal G., Kler P.A. and Berli C.L.A. (2019). Simple method for the assessment of intrinsic kinetic constants in photocatalytic microreactors. *Applied Catalysis B: Environmental*, *241*, 8–17.

Sboui M., Nsib M.F., Rayes A., Swaminathan M. and Houas A. (2017). TiO2–PANI/Cork composite: A new floating photocatalyst for the treatment of organic pollutants under sunlight irradiation. *Journal of Environmental Sciences*, *60*, 3–13.

Shi Z., Zhang Y., Duoerkun G., Cao W., Liu T., Zhang L., Liu J., Li M. and Chen Z. (2020). Fabrication of MoS 2/BiOBr heterojunctions on carbon fibers as a weaveable photocatalyst for tetracycline hydrochloride degradation and Cr (VI) reduction under visible light. *Environmental Science: Nano*, **7(9)**, 2708–2722.

Si C., Zhou J., Gao H., Liu G. and Wu J. (2015). Typical Application of Sound Field in Wastewater Treatment with Fluidized Bed Photocatalytic Reactor. *Water Environment Research*, **87(4)**, 378–383.

Silva P.C., Ferraz N.P., Perpetuo E.A. and Asencios Y.J.O. (2019). Oil produced water treatment using advanced oxidative processes: heterogeneous-photocatalysis and photo-Fenton. *Journal of Sedimentary Environments*, **4(1)**, 99–107.

Singh A.P., Kodan N., Mehta B.R., Held A., Mayrhofer L. and Moseler M. (2016). Band edge engineering in BiVO4/TiO2 heterostructure: enhanced photoelectrochemical performance through improved charge transfer. *ACS Catalysis*, **6(8)**, 5311–5318.

Sood S., Umar A., Mehta S.K. and Kansal S.K. (2015). Highly effective Fe-doped TiO2 nanoparticles photocatalysts for visible-light driven photocatalytic degradation of toxic organic compounds. *Journal of Colloid and Interface Science*, *450*, 213–223.

Sraw A., Kaur T., Pandey Y., Sobti A., Wanchoo R.K. and Toor A.P. (2018). Fixed bed recirculation type photocatalytic reactor with TiO2 immobilized clay beads for the degradation of

pesticide polluted water. *Journal of Environmental Chemical Engineering*, **6(6)**, 7035–7043.

Srikanth B., Goutham R., Narayan R.B., Ramprasath A., Gopinath K.P. and Sankaranarayanan A.R. (2017). Recent advancements in supporting materials for immobilised photocatalytic applications in waste water treatment. *Journal of Environmental Management*, *200*, 60–78.

Tugaoen H.O., Garcia-Segura S., Hristovski K. and Westerhoff P. (2018). Compact light-emitting diode optical fiber immobilized TiO2 reactor for photocatalytic water treatment. *Science of The Total Environment*, *613*, 1331–1338.

Turolla A., Santoro D., de Bruyn J.R., Crapulli F. and Antonelli M. (2016). Nanoparticle scattering characterization and mechanistic modelling of UV–TiO2 photocatalytic reactors using computational fluid dynamics. *Water Research*, *88*, 117–126.

Urkasame K., Yoshida S., Takanohashi T., Iwamura S., Ogino I. and Mukai S.R. (2018). Development of TiO2–SiO2 photocatalysts having a microhoneycomb structure by the ice templating method. *ACS Omega*, **3(10)**, 14274–14279.

Varjani S., Kumar G. and Rene E.R. (2019). Developments in biochar application for pesticide remediation: current knowledge and future research directions. *Journal of Environmental Management*, *232*, 505–513.

Wang B., de Godoi F.C., Sun Z., Zeng Q., Zheng S. and Frost R.L. (2015). Synthesis, characterization and activity of an immobilized photocatalyst: natural porous diatomite supported titania nanoparticles. *Journal of Colloid and Interface Science*, *438*, 204–211.

Wang J., Li X., Ren Y., Xia Z., Wang H., Jiang W., Liu C., Zhang S., Li Z. and Wu S. (2021). The effects of additive on properties of Fe doped TiO2 nanoparticles by modified sol-gel method. *Journal of Alloys and Compounds*, *858*, 157726.

Wang L., Wang X., Yin J., Zhu Y. and Wang C. (2016). Silica induced oxygen vacancies in supported mixed-phase TiO2 for photocatalytic degradation of phenol under visible light irradiation. *Catalysis Communications*, *87*, 98–101.

Wang X. and Lim T.-T. (2010). Solvothermal synthesis of C–N codoped $TiO_2$ and photocatalytic evaluation for bisphenol A degradation using a visible-light irradiated LED photoreactor. *Applied Catalysis B: Environmental*, **100(1–2)**, 355–364.

Wetchakun N., Pirakitikulr P., Chiang K. and Phanichphant S. (2008). Visible light-active nano-sized Fe-doped TiO 2 photocatalysts and their characterization. *2008 2nd IEEE International Nanoelectronics Conference*, 836–841.

Xu Z., Li C., Fu N., Li W. and Zhang G. (2018). Facile synthesis of Mn-doped TiO 2 nanotubes with enhanced visible light photocatalytic activity. *Journal of Applied Electrochemistry*, *48*, 1197–1203.

Zhang H. and Zhu H. (2012). Preparation of Fe-doped TiO2 nanoparticles immobilized on polyamide fabric. *Applied Surface Science*, **258(24)**, 10034–10041.

Zhang K. (2002). Axial solid concentration distribution in tapered and cylindrical bubble columns. *Chemical Engineering Journal*, **86(3)**, 299–307.

Zhang K., Zhao Y. and Zhang B. (2003). Gas holdup characteristics in a tapered bubble column. *International Journal of Chemical Reactor Engineering*, ***1*(1)**.

Zhang K., Zhao Y. and Zhang B. (2004). Hydrodynamic behavior in a tapered bubble column. *Chemical Research in Chinese Universities*, **20(4)**, 478–482.

Zhang S., Zhang J., Sun J. and Tang Z. (2020). Capillary microphotoreactor packed with TiO2-coated glass beads: An efficient tool for photocatalytic reaction. *Chemical Engineering and Processing-Process Intensification*, ***147***, 107746.

Zhang Y., Shen Y., Gu F., Wu M., Xie Y. and Zhang J. (2009). Influence of Fe ions in characteristics and optical properties of mesoporous titanium oxide thin films. *Applied Surface Science*, **256(1)**, 85–89.

Zhu J., Ren J., Huo Y., Bian Z. and Li H. (2007). Nanocrystalline Fe/TiO2 visible photocatalyst with a mesoporous structure prepared via a nonhydrolytic sol− gel route. *The Journal of Physical Chemistry C*, **111(51)**, 18965–18969.